

Estimation of Near-Surface Air Temperature Lapse Rate Based on MODIS Data Over the Tibetan Plateau

Hailing Zhong , Ji Zhou , Senior Member, IEEE, Wenbin Tang, Guiyun Zhou , Ziwei Wang, Wei Wang , Yizhen Meng, and Jin Ma , Member, IEEE

Abstract—Near-surface air temperature lapse rate (NSATLR) is one of the key criteria for judging atmospheric stability. It is an important model parameter in glacier, hydrology, ecology, climate, and meteorology in high mountains such as the Tibetan Plateau (TP). However, due to the complex interaction between the atmosphere and land surface, retrieving NSATLR from remotely sensed data is challenging. In this article, we develop a novel model based on the MODIS data to estimate the daily 5-km NSATLR over the TP. The input parameters of the model include digital elevation model and the near-surface air temperature estimated from the MODIS data. By combining moving window and specified criteria, the pixel-based NSATLR with a 5-km spatial resolution over the TP is estimated. In addition, we also estimate the NSATLR based on the meteorological data over the TP (NSATLR_{in situ}) to evaluate the accuracy of NSATLR estimation model. Results demonstrate that the NSATLR estimate agrees well with NSATLR_{in situ} in the eastern TP, with an overall root-mean-square error of 1.51 °C/km and a mean bias error of −0.78 °C/km. Larger deviation exists in the southern TP. Thanks to the evident advantages of simplicity, the availability of input parameters and the independence from the meteorological data, the developed model can be applied to larger areas.

Index Terms—Lapse rate, meteorological data, MODIS, near-surface air temperature, Tibetan Plateau.

I. INTRODUCTION

NEAR-SURFACE air temperature lapse rate (NSATLR) refers to the lapse rate of near-surface air temperature (NSAT) decreases with altitude. It is generally assumed that the NSAT decreases by 6.5 °C for per kilometer increase in altitude [1], [2], [3], whereas NSAT in the real atmosphere does not always decrease at a constant rate. For example, with the phenomenon of temperature inversion, NSAT increases with altitude [4]. In recent decades, with the intensification of global warming, the glacier melting has accelerated, and the amount of ice-snow melting water has increased. The NSAT, which is directly related to global warming, has become a research focus [5].

Manuscript received 10 February 2023; revised 28 March 2023; accepted 20 April 2023. Date of publication 26 April 2023; date of current version 22 May 2023. This work was supported in part by the National Natural Science Foundation of China under Grant 42271387 and Grant 42201417 and in part by ESA-MOST Dragon 5 Cooperation Programme under Grant 59318. (Corresponding authors: Ji Zhou; Guiyun Zhou.)

The authors are with the School of Resources and Environment, University of Electronic Science and Technology of China, Chengdu 611731, China (e-mail: zhonghailing177@163.com; jzhou233@uestc.edu.cn; wenbint@stu.uestc.edu.cn; zhongguiyun@uestc.edu.cn; wangzw@std.uestc.edu.cn; wangw@std.uestc.edu.cn; yz.meng@std.uestc.edu.cn; jin.ma@uestc.edu.cn).

Digital Object Identifier 10.1109/JSTARS.2023.3270560

Due to the unique geographical conditions and complex natural environment, the Tibetan Plateau (TP) has an important impact on the climate change in its surroundings and even the world [5], [6]. NSATLR can be used to analyze the spatial distribution characteristics of NSAT and simulate the surface environment in mountainous areas such as the TP. Investigations on the surface environment of the TP are of great significance to climate change studies but they only hold scarce scientific data [7]. The spatially continuous NSATLR can provide more accurate parameters for glacier study, hydrological, and ecological simulations [8], [9], [10], thus making possible more comprehensive theoretical study for examining the fragile ecosystem of the TP. In addition, the investigation of NSATLR can also improve the accuracy of regional NAST downscaling [11], and provide input data support for the development of NSAT datasets with high spatial resolutions.

At present, the commonly used NSATLR estimation method is simple linear regression based on in situ NAST and elevation [12], [13]. In addition, there are also a few studies using multiple linear regression models to estimate NSATLR. In a multiple linear regression model, NSAT is the dependent variable, and elevation, longitude, latitude, and other parameters are the independent variables, and the coefficient of elevation is used as NSATLR [14]. For large areas with complex terrain and climate conditions, meteorological stations are usually divided into several subregions according to specific rules (e.g., longitude, latitude, and climate), and the overall NSATLR of each subregion is calculated, respectively [7], [15]. A few studies have reported the estimation of NSATLR by using meteorological data around the TP [16], [17], [18]. In general, the NSATLR over the TP has strong seasonal characteristics, with shallow NSATLR in summer and steep NSATLR in winter [19], [20]. Guo et al. [21] showed that the annual average NSATLR in the TP was 5.9 °C/km. A bimodal seasonal pattern was found in the Himalayas, with two maximum values before and after the monsoon [22]. However, the above NSATLR estimation methods can only obtain the NSATLR at stations, which cannot describe the spatially continuous NSATLR for large areas. In addition, due to the vast area and complex geographical environment of the TP, it is very difficult to construct enough number of meteorological stations. Therefore, the representativeness of NSATLR estimates based on meteorological data is particularly insufficient.

With the continuous development of remote sensing technology, the scientific communities have applied satellite thermal infrared remote sensing to obtain large scale NSAT data,

which provides the possibility for obtaining spatially continuous NSATLR. For example, Wang et al. [23] used the NSAT data estimated by MODIS surface temperature and elevation data to conduct regression analysis within a $10\text{ km} \times 10\text{ km}$ moving window. It was found that the NSATLR at nighttime in the northern and central parts of the TP was lower than that at daytime, but the NSATLR at daytime in the eastern part of the TP and the Hengduan Mountains was lower than that at nighttime. At present, most of the methods based on remotely sensed thermal infrared surface temperature data to estimate NSAT use elevation as a universal input parameter [24], [25]. In addition, NSATLR, as the regression coefficient of elevation in the NSAT estimation models, has been indirectly included in the process of estimating NSAT. Therefore, most of the NSAT products based on remotely sensed thermal infrared surface temperature estimation cannot be used to estimate NSATLR. In the process of estimating NSAT based on remotely sensed thermal infrared surface temperature data, most methods use a variety of surface variables and in situ NAST data as auxiliary parameters to achieve accurate NAST estimates [5], [26]. MODIS atmospheric profile products have potential advantages in estimating NSAT, which do not depend on auxiliary surface variables and in situ NSAT data. Therefore, it is worthy to explore the possibility of using the MODIS atmospheric profile product to obtain NSAT of the TP and provide input data support for the NSATLR estimation.

In this context, this article develops a novel model for estimating NSATLR from MODIS atmospheric profile product, and produces 5-km daily NSATLR over the TP from 2010 to 2019. The input parameters of the model include the elevation data and MODIS atmospheric profile product, and the NSATLR is estimated by combining moving window and specified criteria. In the process of estimating NSATLR, the size of the moving window is constantly changed to satisfy specified criteria, thus, strictly controlling the input data of the model to obtain more credible NSATLR values. In addition, since NSATLR cannot be obtained directly from in situ data, the estimated NSATLR lacks valid validation datasets. Therefore, we also estimate NSATLR from the ground measurements at 86 stations in the TP. The NSATLR estimates based on in situ data is hereinafter referred to as $\text{NSATLR}_{\text{in situ}}$. The NSATLR estimate is then compared with $\text{NSATLR}_{\text{in situ}}$ to verify the effectiveness of the NSATLR estimation model.

II. STUDY AREA AND MATERIALS

A. Study Area

As described previously, the area under examination in this article is the TP ($25^\circ - 40^\circ\text{N}$, $75^\circ - 105^\circ\text{E}$). The huge mountains and high-altitude characteristics of the TP have a significant impact on the climate of Asia and even around the world. The terrain of the mountains is complex and the vertical throw is large (see Fig. 1), resulting in complex and diverse vertical changes of temperature. The average altitude of the TP is more than 4 km. Thus, the TP is known as the “third pole” in the world and plays an important role in the global climate and atmospheric circulation.

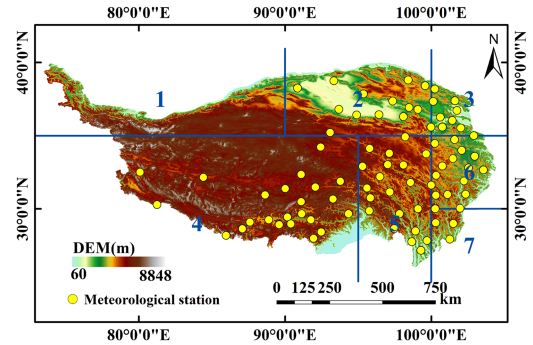


Fig. 1. Distribution of CMA stations and elevation of the TP. The divided seven areas are also shown.

TABLE I
DIVISION OF SEVEN SUBREGIONS IN THE TP (ACCORDING TO [15])

Area	Longitude range	Latitude range
Area 1	$73^\circ - 90^\circ\text{E}$	$35^\circ - 40^\circ\text{N}$
Area 2	$90^\circ - 100^\circ\text{E}$	$35^\circ - 40^\circ\text{N}$
Area 3	$100^\circ - 105^\circ\text{E}$	$35^\circ - 40^\circ\text{N}$
Area 4	$78^\circ - 95^\circ\text{E}$	$27^\circ - 35^\circ\text{N}$
Area 5	$95^\circ - 100^\circ\text{E}$	$27^\circ - 35^\circ\text{N}$
Area 6	$100^\circ - 107.5^\circ\text{E}$	$30^\circ - 35^\circ\text{N}$
Area 7	$100^\circ - 105^\circ\text{E}$	$25^\circ - 30^\circ\text{N}$

Due to the complex topography and diverse climate changes on the TP, validation analysis of NSATLR in different subregions is required. Li et al. [15] divided the TP into seven subregions in their study of NSATLR in mainland China (see Fig. 1), and the division of these subregions is shown in Table I. Under this division framework, each subregion has similar climatic characteristics and certain elevation variations. The same division framework is used in this article to divide the meteorological stations on the TP into seven subregions, and only six subregions are used in this article because no meteorological stations exist in Area 1.

B. Datasets

1) *MODIS Data*: MODIS is an important sensor on board the earth observation system (EOS) Terra and Aqua satellites. A dedicated research showed that the NSAT retrieval from Terra MODIS data is more accurate than that of Aqua MODIS data [27]. Thus, we use the MODIS atmospheric profile product (MOD07_L2) derived from the Terra MODIS data in this article. This product has a spatial resolution of 5-km. Specifically, the atmospheric temperature profiles and pressure levels included in MOD07_L2 atmospheric product are used in this article. From the atmospheric temperature profiles, atmospheric temperatures at 20 vertical atmospheric pressure levels are available, namely 1000, 950, 920, 850, 780, 700, 620, 500, 400, 300, 250, 200, 150, 100, 70, 50, 30, 20, 10, and 5 hPa. Affected by the

cloud contamination, the MOD07_L2 product can only provide the atmospheric temperature profile and pressure levels under clear-sky conditions. The MOD07_L2 products from 2010 to 2019 are provided by the U.S. Geological Survey Land Process Distributed Active Archive Center (<https://search.earthdata.nasa.gov>).

2) *Meteorological Data*: In this article, the average daily in situ NAST, sunshine hours, evapotranspiration, wind speed and relative humidity provided by China Meteorological Administration (CMA, <http://data.cma.cn/>) are used. The time range is from 2010 to 2019, and the temporal resolution is daily. The NAST is measured at 2 m above the ground surface. According to the extent of the TP, a total of 86 meteorological stations, of which more than 70% are distributed in the eastern and southern regions of the TP, are selected in this article. A reliable NSATLR_{in situ} estimation requires enough stations. Therefore, this article mainly uses the in situ NSAT data in the eastern and southern regions of the TP, which have relatively dense distribution of stations. The station distribution is shown in Fig. 1.

3) *Digital Elevation Model*: Digital elevation model (DEM) is a digital simulation of terrain through elevation data. It is an entity ground model that represents ground elevation in the form of a set of ordered numerical arrays. The DEM dataset, with a 90-m spatial resolution, are produced by the shuttle radar topography mission (SRTM). The DEM dataset can be obtained from the United States Geological Survey FTP site (<https://srtm.csi.cgiar.org/>) or the spatial information consortium.

III. METHODOLOGY

The estimation of NSATLR based on the MODIS atmospheric profile product (i.e., MOD07_L2) includes two steps. The first one is to determine the pixel-based NSAT from the MOD07_L2 product using the parameterization scheme. The second one is to estimate the pixel-based NSATLR based on the NSAT and elevation using moving window. At the same time, the daily NSATLR_{in situ} at 86 stations over the TP is used as validation data to explore the credibility of NSATLR estimation model.

A. Calculation of NSATLR_{in situ} Based on the in situ Measurements

As described previously, the commonly used NSATLR estimation methods include multiple linear regression in addition to simple linear regression. The simple linear regression refers to a linear regression of NSAT on elevation

$$T_a = a \times Z + b \quad (1)$$

where T_a is the NSAT; Z is elevation; a and b are regression coefficients and a is the estimated NSATLR.

The multiple linear regression refers to the establishment of multiple regression models with NSAT as the dependent variable and multiple independent variables such as altitude, longitude, and latitude

$$T_a = a_0 + a_1 \times Z + a_2 \times Lon + a_3 \times Lat \quad (2)$$

where Lon is longitude, Lat is latitude; a_0 , a_1 , and a_2 are regression coefficients, and a_0 is the estimated NSATLR.

One should note that the independent variables used in the multiple linear regression model may have multiple collinearity, which makes the coefficient of elevation in the regression equation unstable. The multicollinearity test is realized by calculating the variance expansion factor (VIF). When the VIF value is higher than 5, it is considered that the multicollinearity of independent variables is serious. In this article, the multicollinearity test is carried out based on the in situ NSAT to determine whether it is feasible to use multiple linear regression model to estimate NSATLR_{in situ} in the TP.

The estimation of NSATLR_{in situ} needs to be conducted separately for each station. First, the spatial distances between the station under examination and other stations are calculated, and 15 to 25 neighboring stations are selected. Second, the NSAT and elevation at 15 stations are linearly regressed to determine whether they reached the significance level (0.1). If the evaluation standard of significance level (0.1) is satisfied, the regression coefficient of elevation is taken as the final NSATLR_{in situ} of the station. Otherwise, the number of neighboring stations is increased until the significance level meets the requirements. If the significance level is still unqualified when the number of neighboring stations exceeds 25, the station under examination does not have a valid NSATLR_{in situ} value. Finally, NSATLR_{in situ} of each station is obtained by repeating this process.

B. Estimation of NSATLR Based on MODIS Atmospheric Profile Product

1) *Determination of NSAT From MOD07_L2 Product*: First, the NSAT over the TP is determined using the MOD07_L2 product. An atmospheric temperature profile of the MOD07_L2 product has 20 vertical atmospheric pressure levels, but there is no corresponding relationship between the air temperature and NSAT. The parameterization scheme for determining NSAT here is based on the troposphere hydrostatic atmospheric assumption. Specifically, the atmospheric pressure levels and temperature profiles provided by the MOD07_L2 product are used to determine the NSAT according to the fact that the temperature changes with the increase of altitude in most cases [28], [27]

$$T_{a1} = T_a^{L1} + \frac{ALR}{\rho g} (P^{L1} - P^S) \quad (3)$$

where T_{a1} is the NSAT estimated by MOD07_L2 product; P^{L1} is the pressure level closest to the surface; P^S is the surface pressure level provided by MOD07_L2 product; T_a^{L1} is the atmospheric temperature corresponding to P^{L1} ; ρ is the air density; g is the gravitational acceleration; and ALR is the adiabatic lapse rate.

According to the two pressure levels close to the ground in the MOD07_L2 product, the troposphere hydrostatic atmospheric assumption can be written as

$$\frac{P^{L2} - P^{L1}}{\Delta H} = -\rho g \quad (4)$$

where P^{L2} is the pressure level above P^{L1} , and ΔH is the elevation difference between two atmospheric pressure levels.

The ALR is retrieved from two pressure levels closest to the ground of the MOD07_L2 atmospheric product as follows:

$$\text{ALR} = \frac{T_a^{\text{L2}} - T_a^{\text{L1}}}{\Delta H} \quad (5)$$

where T_a^{L2} is the atmospheric temperature corresponding to P^{L2} . Combining (3), (4), and (5), NSAT can be calculated as

$$T_{a1} = T_a^{\text{L1}} + \frac{T_a^{\text{L2}} - T_a^{\text{L1}}}{P^{\text{L2}} - P^{\text{L1}}}(P^{\text{S}} - P^{\text{L1}}). \quad (6)$$

All variables required by (6) can be obtained from the MOD07_L2 atmospheric profile product. Thus, without any ancillary data, the NSAT under clear-sky conditions can be retrieved based completely on the MOD07_L2 product.

MODIS atmospheric profile product estimates the instantaneous NSAT, including NSAT at multiple times of day and night. This study uses MOD07_L2 product to estimate the instantaneous temperatures at multiple moments in a diurnal cycle (10:30 and 22:30 local solar time), and then averages them to obtain the daily average NSAT. MOD07_L2 product and the process of estimating NAST have uncertainties [30], [30]. Hence, the estimated NAST needs to be further processed.

Zhu et al. [27] evaluated the reliability of MODIS atmospheric profile product for estimating NSAT in two completely different regions. The results showed that the NSAT estimated by MODIS atmospheric profile product was underestimated compared with the in situ NSAT, while the surface temperature obtained from MODIS cloud products was overestimated. Therefore, the NSAT with higher accuracy can be obtained by averaging the two products. According to this finding, this article uses this averaging scheme to obtain more accurate NSAT. The formula is as follows:

$$T_a = \frac{T_{a1} + T_s}{2} \quad (7)$$

where T_a is the NSAT estimated by the averaging scheme; T_{a1} is the NSAT estimated by the MOD07_L2 atmospheric profile product; and T_s is the surface temperature provided by the MOD07_L2 product.

2) *Estimation of NSATLR Based on Pixel-Based NSAT*: Considering NSATLR is more accurate in local areas, this article uses a moving window approach to estimate NSATLR pixel by pixel. The pixel values in the moving window need to meet the following criteria for the estimation of NSATLR: 1) NSAT is highly correlated with elevation, and the significance level is within 0.1; 2) there is a certain elevation difference in the moving window and it is generally believed that when the elevation difference is larger than 10 m, the estimated NSATLR is credible; and 3) the number of effective pixels accounts for more than half of the number of pixels in the moving window. When estimating the NSATLR value pixel by pixel, it is necessary to determine whether the pixel value in the moving window meets the above criteria. If not, the size of the moving window is incrementally increased from 5×5 to 15×15 at a step of 2×2 until the pixel value in the moving window meets the required criteria, and the optimal moving window size is obtained. Then, NSATLR value of the central pixel of the moving window is obtained by linear regression of the NSAT and elevation in the moving window.

The abovementioned process is repeated for each effective pixel to generate a daily spatially continuous NSATLR in the TP. It is worth noting that when using the data on DOY 90, 180, 270, and 360 of 2010 to carry out the test of moving window size, we found that more than 80% of the pixels met the several criteria of NSATLR estimation when the moving window is 5×5 , whereas less than 2% of the pixels met the criteria when the moving window is more than 15×15 . Therefore, considering the distance between pixels and test results, the moving window is selected from 5×5 to 15×15 at a step of 2×2 .

3) *Evaluation Strategy*: First, the accuracy of daily NSAT based on MOD07_L2 is evaluated using daily in situ NSAT collected from 86 ground stations over the TP from 2010 to 2019. The evaluation indexes of NSAT include mean bias error (MBE), RMSE, and coefficient of determination (R^2).

Second, the accuracy of NSATLR is examined from two aspects: 1) comparative analysis of NSATLR_{in situ} and NSATLR to evaluate the effectiveness of NSATLR estimation model; and 2) NSATLR is analyzed from the temporal and spatial characteristics, and compared with previous research to further evaluate the reliability of NSATLR estimated in this article.

IV. RESULTS

A. Estimated NSATLR_{in situ}

The results of multicollinearity test of 86 stations in the TP show that there is serious multiple collinearity in the process of using multiple linear regression method to estimate NSATLR when elevation, longitude, and latitude are used as independent variables. Here, results of DOY 90, 180, 270, and 360 of 2010 are taken as examples. On DOY 90, there are 36 stations with the VIF value of latitude independent variable greater than 5 (the maximum value is 22.01), and 33 stations with the VIF value of longitude independent variable greater than 5 (the maximum value is 41.41). On DOY 180, there are 27 stations with the VIF value of latitude independent variable greater than 5 (the maximum value is 183.92), and 23 stations with the VIF value of longitude independent variable greater than 5 (the maximum value is 90.47). On DOY 270, there are 31 stations with the VIF value of latitude independent variable greater than 5 (the maximum value is 232.52), and 27 stations with the VIF value of longitude independent variable greater than 5 (the maximum value is 90.47). On DOY 360, there are 22 stations with the VIF value of latitude independent variable greater than 5 (the maximum value is 26.63), and 21 stations with the VIF value of longitude independent variable greater than 5 (the maximum value is 129.04). Therefore, this article uses the simple linear regression method to estimate the NSATLR.

Fig. 2 shows the spatial distribution of NSATLR_{in situ} in four seasons from 2010 to 2019. Overall, the average NSATLR_{in situ} in spring (March to May), summer (June to August), autumn (September to November), and winter (December to February) are concentrated in the range of 0.45–9.34 °C/km, 0.44–6.86 °C/km, 0.45–8.89 °C/km, and 0.35–9.04 °C/km, respectively. Fig. 3 shows the spatial distribution NSATLR_{in situ} on DOY 90, 180, 270, and 360 of 2010. Similar to the spatial distribution characteristics of NSATLR_{in situ} in four seasons,

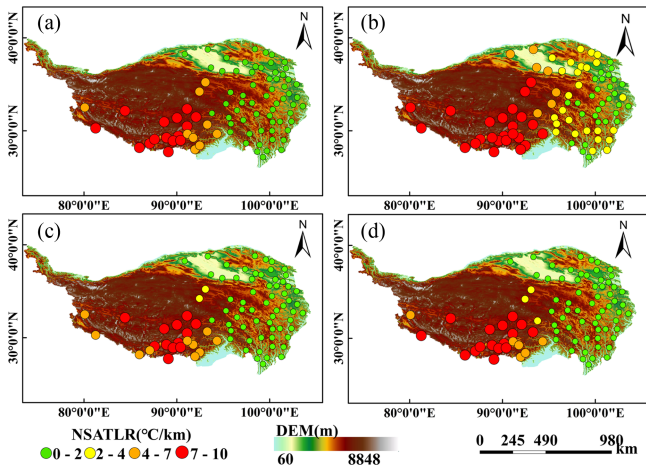


Fig. 2. Spatial distribution of the average NSATLR_{in situ} in the four seasons from 2010 to 2019. (a) Spring. (b) Summer. (c) Autumn. (d) Winter.

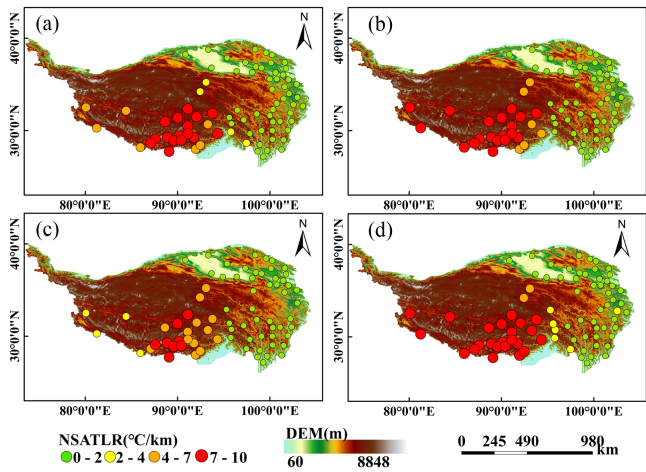


Fig. 3. Spatial distribution of the NSATLR_{in situ} on DOY 90, 180, 270, and 360 of 2010. (a) DOY 90. (b) DOY 180. (c) DOY 270. (d) DOY 360.

the southern and western NSATLR_{in situ} are deeper than the eastern NSATLR_{in situ}. On day 270, the deeper NSATLR_{in situ} are the least, and on day 360, the deeper NSATLR_{in situ} are the most.

Fig. 4 shows the overall monthly variation characteristics of NSATLR_{in situ} from 2010 to 2019. In general, the NSATLR_{in situ} in the central and southwestern parts of the TP are higher than those in the eastern part. The NSATLR_{in situ} in winter and spring is deeper, and the NSATLR_{in situ} in summer and autumn is shallower.

B. Estimated NSAT Based on MODIS Data

According to the atmospheric pressure levels and temperature profiles provided by MOD07_L2 product, the NSAT of the TP from 2010 to 2019 is estimated. The in situ NSAT data are used to examine the estimated NAST. The results are shown in Fig. 5. The estimated NSAT and the in situ NSAT have R^2 of 0.50–0.60, RMSE of 5.62–5.99 °C, and MBE of –1.74 to

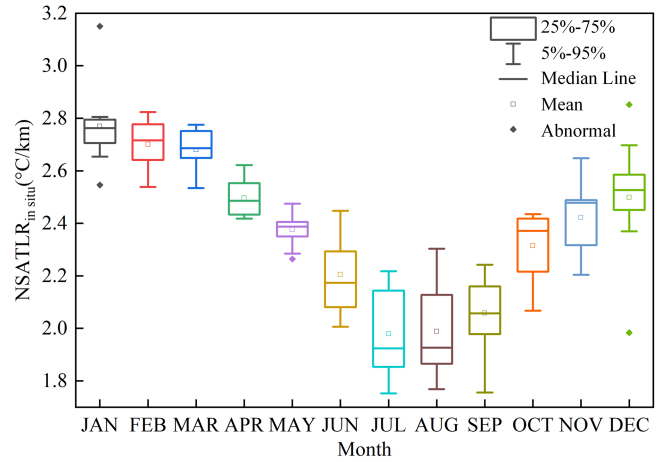


Fig. 4. Monthly variations of NSATLR_{in situ} from 2010 to 2019.

0.55 °C. Except for the positive value in 2010, the MBE are negative from 2011–2019, indicating that the estimated NSAT is lower than the in situ NSAT. This is because the atmospheric pressure levels used to estimate NSAT is lower than the surface pressure. The atmospheric profile extrapolation can reduce the underestimation by hydrostatic interpolation, but there are still some errors. It is worth noting that there is a large deviation between the NSAT of the TP directly estimated by MOD07_L2 product and the in situ NSAT. Therefore, the averaging scheme is needed to further address the NSAT.

Fig. 6 shows the overall performance of the estimated NSAT after using the averaging scheme [namely, (7)]. The estimated NSAT and the in situ NSAT have R^2 of 0.80 to 0.84, RMSE of 3.90 to 4.48 °C, and MBE of 1.52–2.46 °C. The accuracy of NSAT after using the averaging scheme has been improved to some extent. The improved NSAT can be used to estimate NSATLR.

C. Estimated NSATLR Based on MODIS Data

1) *Evaluation of the Estimated NSATLR:* Based on the NSATLR estimation model, we estimate the daily NSATLR in the TP from 2010 to 2019. In this article, the remotely sensed NSATLR is compared with the NSATLR_{in situ} at meteorological stations to evaluate the accuracy of the NSATLR estimation model.

The NSATLR_{in situ} values of the six subregions are compared with the estimated NSATLR. As shown in Fig. 7, the RMSEs in Area 6 and Area 7 are smaller than those in other areas; the RMSE of Area 4 is the largest with a value range of 2.20–2.92 °C/km. In general, the RMSE value in the west is larger with multiyear average value of 2.53 °C/km. The RMSE in the central and eastern TP is lower with multiyear average value of 1.38 °C/km.

The MBE value of the Area 4 is positive, ranging from 1.44 to 2.35 °C/km and the multiyear average value is 2.01 °C/km, indicating the estimated NSATLR is higher than the NSATLR_{in situ} in Area 4. The MBE of Area 2 is larger, ranging from 1.91 to 1.42 °C/km and the MBE of Area 6 is the smallest, ranging

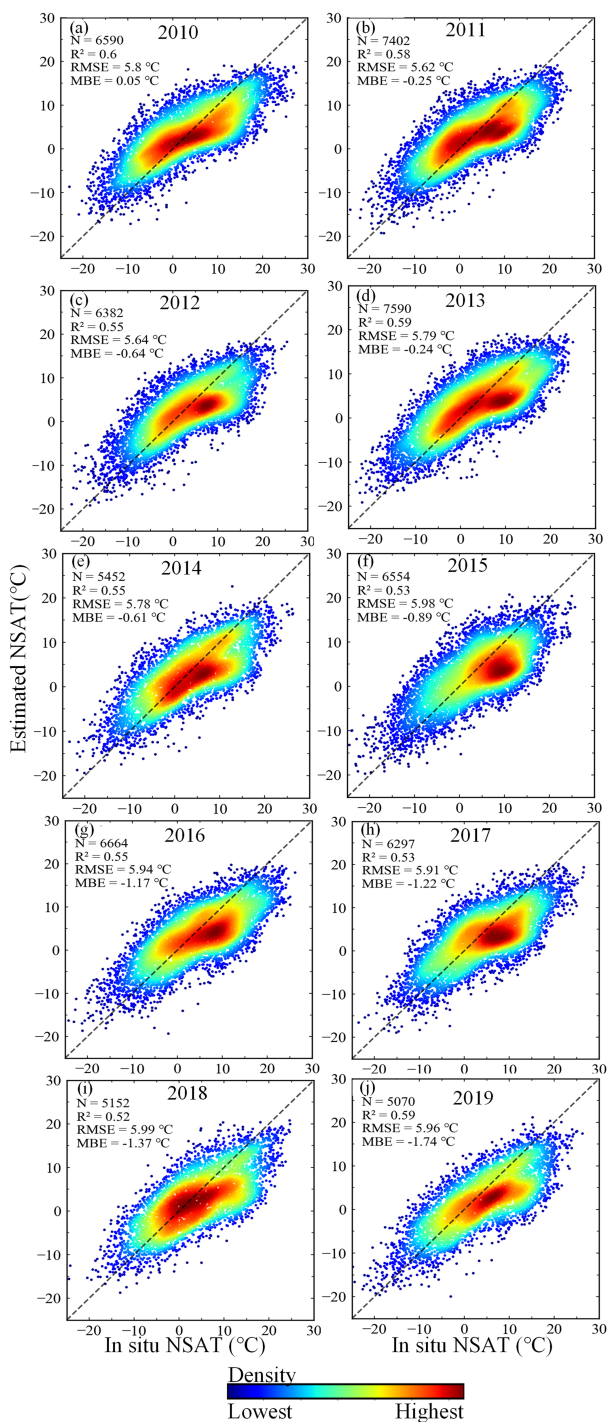


Fig. 5. Density plots between the in situ NSAT and the estimated NSAT based on the MOD07_L2 product from 2010 to 2019.

from 1.04 to 0.71 °C/km. It is worth noting that the MBE values of subregions except Area 4 are all negative, indicating that the estimated NSATLR in this article is higher than the NSATLR_{in situ} in most areas of the TP.

2) *Time Series Analysis*: To explore the temporal variation characteristics of NSATLR and NSATLR_{in situ} in the TP, the number of pixels with effective NSATLR values and the location of station are comprehensively considered and five stations are

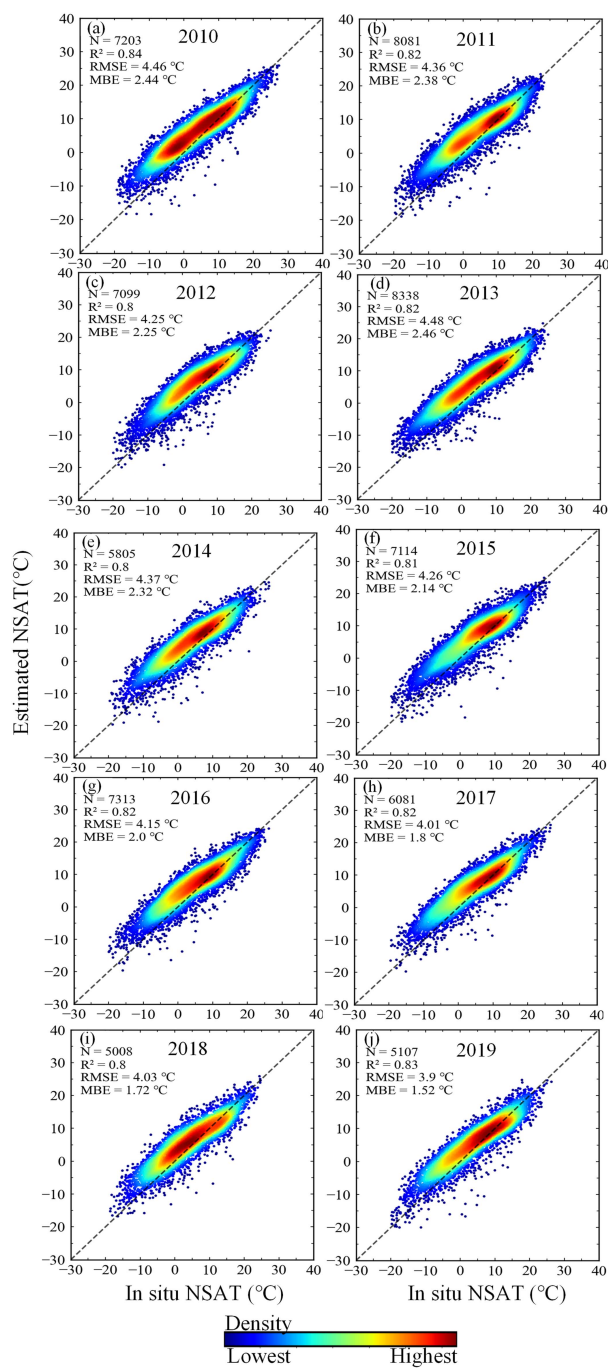


Fig. 6. Density plots between the in situ NSAT and the estimated NSAT based on the averaging scheme from 2010 to 2019.

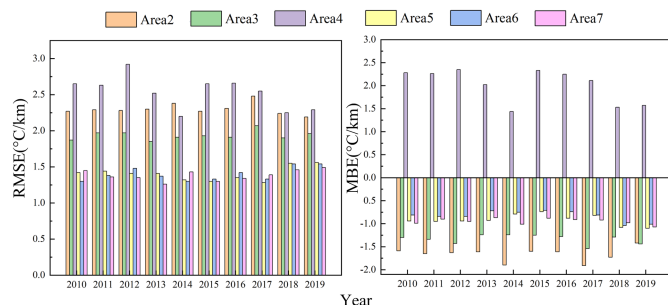


Fig. 7. RMSE and MBE of six subregions in the TP.

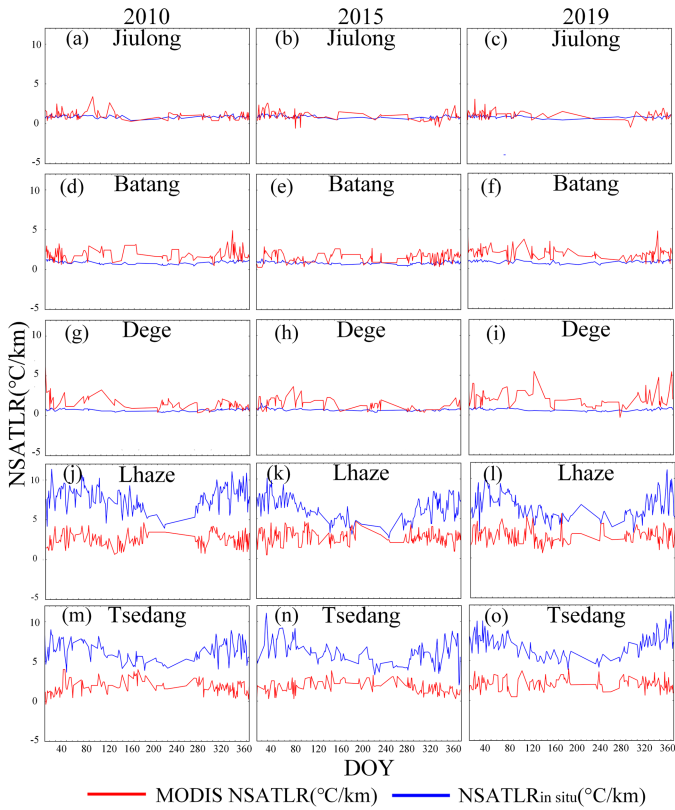


Fig. 8. Time series of NSATLR and NSATLR_{in situ} at the five stations in 2010, 2015, and 2019.

selected for analysis. These five stations are: Jiulong (29°N, 87.6°E), Batang (30°N, 99.1°E), Dege (31.8°N, 98.58°E), Lhaze (29.08°N, 99.1°E), and Tsedang (29.25°N, 91.77°E). Among them, Jiulong, Batang, and Dege are distributed in the eastern TP, while Lhaze and Tsedang are distributed in the central and southern TP. This article extracts daily NSATLR_{in situ} and corresponding NSATLR from five stations in 2010, 2015, and 2019 for the time series analysis.

It can be seen from Fig. 8 that the NSATLR_{in situ} and NSATLR values of Jiulong, Batang, and Dege stations have little difference and have no obvious seasonal characteristics. NSATLR_{in situ} are generally lower than NSATLR at the above three stations. The change range of NSATLR_{in situ} is small for many years, while the change range of NSATLR is large. The values of NSATLR and NSATLR_{in situ} at Lhaze and Tsedang stations are quite different. Since NSATLR_{in situ} is more accurate in local areas, the estimated NSATLR_{in situ} is credible when the number of adjacent pixels or stations is enough. There are more and denser stations in the eastern TP, and the estimated NSATLR_{in situ} are small and close to NSATLR. The number of stations in the central and southern TP is small and sparse, so that the estimated NSATLR_{in situ} are large [15], [23], which is quite different from NSATLR.

3) *Temporal and Spatial Distribution Characteristics*: Fig. 9 shows the spatial distribution of the annual average NSATLR in the TP from 2010 to 2019. The NSATLR has obvious temporal and spatial characteristics. The annual average NSATLR in most areas of the TP are concentrated in 1–8 °C/km. Meanwhile, it is

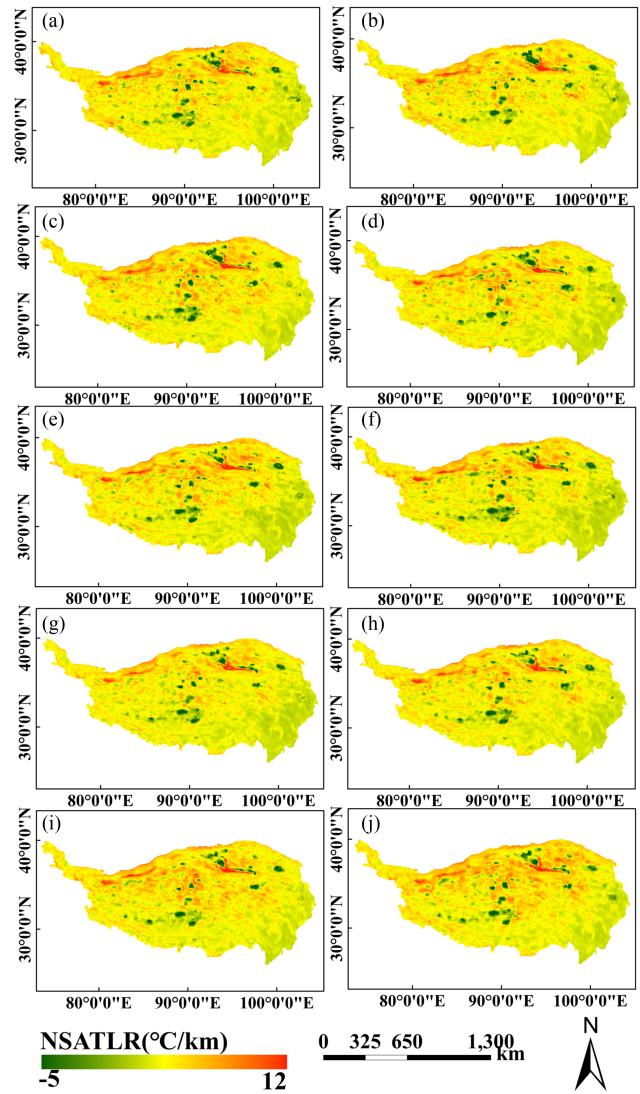


Fig. 9. Spatial distribution of annual average NSATLR from 2010 to 2019. (a) 2010, (b) 2011, (c) 2012, (d) 2013, (e) 2014, (f) 2015, (g) 2016, (h) 2017, (i) 2018, (j) 2019.

basically consistent with the conclusions of previous researches. For example, Kattel et al. [22] showed that the monthly average NSATLR of the Himalayas in the southern TP varies from 3.4 to 5.6 °C/km. He and Wang [18] showed that the monthly average NSATLR of the TP varies from 3 to 7 °C/km. The deep NSATLR pixels are mainly concentrated in the northern, southwestern and central parts of the TP, while the shallow NSATLR pixels are mainly concentrated in the southeastern part of the TP. It can be seen from Fig. 1 that those regions have low altitudes and complex terrain. In 2010, 2018, and 2019, there are more pixels with deep NSATLR values. While in 2014 and 2015, there are more pixels with shallow NSATLR values and those pixels are mainly concentrated in the southeast. In general, the NSATLR and NSATLR_{in situ} have similar spatial distribution characteristics.

Fig. 10 shows the spatial distribution of average NSATLR over the TP in spring, summer, autumn and winter in 2010, 2015 and 2019, respectively. In spring, the year of 2018 has the largest

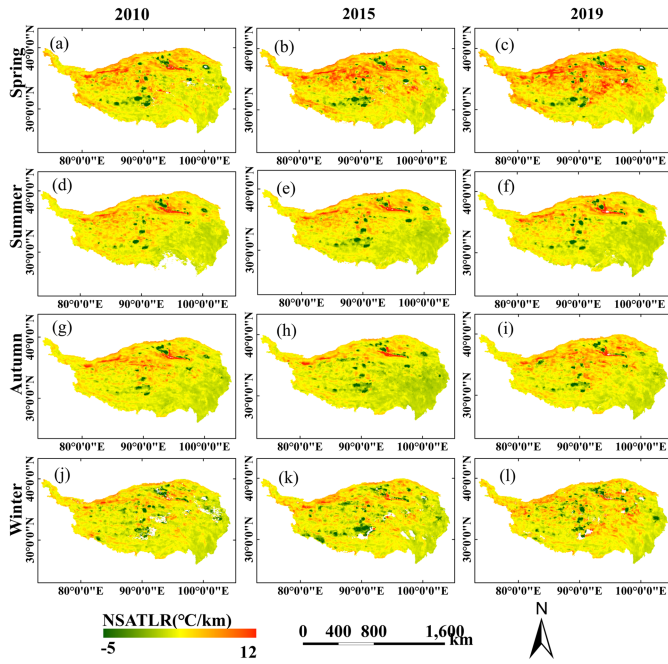


Fig. 10. Spatial distribution of seasonal average NSATLR over the TP.

number of deep NSATLR pixels, followed by 2015 and 2010. In summer, the number of pixels with deep NSATLR in 2015 and 2019 is more than that in 2010. The shallow NSATLR values of the southeastern and eastern TP increase in comparison with the spring. Li et al. [31] and Kattel et al. [12] pointed out that the shallow NSATLR of the southeastern TP in summer may be caused by the Indian monsoon. Summer monsoons from the Indian Ocean bring sufficient moisture to the plateau, forming more clouds and rainfall in the southeastern TP. This leads to an increase in reflected solar radiation and the release of latent heat at high altitudes, resulting in an increase in temperature, thus narrowing the temperature difference between low and high altitudes, leading to a shallower NSATLR. In autumn, there are more pixels with shallow NSATLR in 2010 and 2019 than in 2015. Compared with spring and summer, the number of pixels with shallow NSATLR over the TP increases in autumn. In winter, the year of 2019 has more pixels with deep NSATLR, followed by 2010 and 2015. In general, the NSATLR of the TP is deeper in spring and winter than in summer and autumn. Therefore, NSATLR and NSATLR_{in situ} have similar temporal distribution characteristics.

In some small areas of the TP, the inversion phenomena occur all around the year. According to the online high-resolution map, these small regions are mostly lakes or basins. These small regions are more prone to deep inversion in summer, while in spring, autumn and winter, the number of regions with inversion phenomena decreases and the inversion value becomes shallow. This may be due to the high altitudes and some snow areas of the TP. As temperature rises and snow melts in summer, cold air accumulation at lower altitudes and warm airflow at higher altitudes are more exposed to these more complex terrains, leading to such inversions phenomena [32]. In addition, this may also

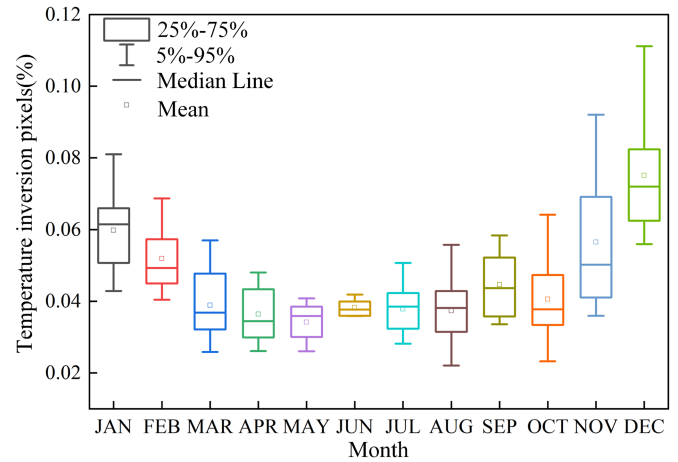


Fig. 11. Percentage of inversion pixels for 12 months from 2010 to 2019.

be related to local topographic conditions and meteorological factors [15].

Fig. 11 shows the percentage of inversion pixels over the TP for 12 months from 2010 to 2019. Except for the abnormal values, the percentage of inversion pixels in the TP is no more than 12% and no less than 2%. Overall, the percentage of inversion pixels in spring and winter is higher than in summer and autumn, which is consistent with previous studies [12], [33], [34]. Among them, the percentage of inversion pixels in spring and winter is higher, and the range is 2.6%–8.1% and 2.3%–11.1%, respectively. The percentage range of inversion pixels in summer is 2.6%–4.8%. The percentage of inversion pixels in autumn is the smallest, with the range of 2.2%–5.8%. In addition, the proportions of inversion pixels in the three seasons are relatively stable except for the larger proportion of inversion pixels in winter.

D. Analysis of the Relationship Between NSATLR and Meteorological Factors

To further explore the relationship between NSATLR and multiple meteorological factors, this article analyzes the correlation between NSATLR and sunshine hours, evapotranspiration, wind speed, and relative humidity (see Fig. 12).

There is a positive correlation between sunshine hours and NSATLR. Sunshine hours represent the energy of solar radiation, which is incident to the ground through the atmosphere. Some of its energy is reflected and some is absorbed by the ground and the atmosphere. The near surface atmosphere also obtains heat from the ground. However, the atmosphere on the TP is thin, which is not conducive to the preservation of heat and dissipates more heat. In spring, summer, autumn and winter of 2010 to 2019, the mean correlation coefficients between sunshine hours and NSATLR are 0.19, 0.21, 0.12, and 0.27, respectively. The correlations between sunshine hours and NSATLR are stronger in winter and weaker in autumn.

There is a positive correlation between the surface evapotranspiration and NSATLR. Evapotranspiration is the process of surface soil and vegetation transporting water vapor to the atmosphere, which is a complex physical and biological process.

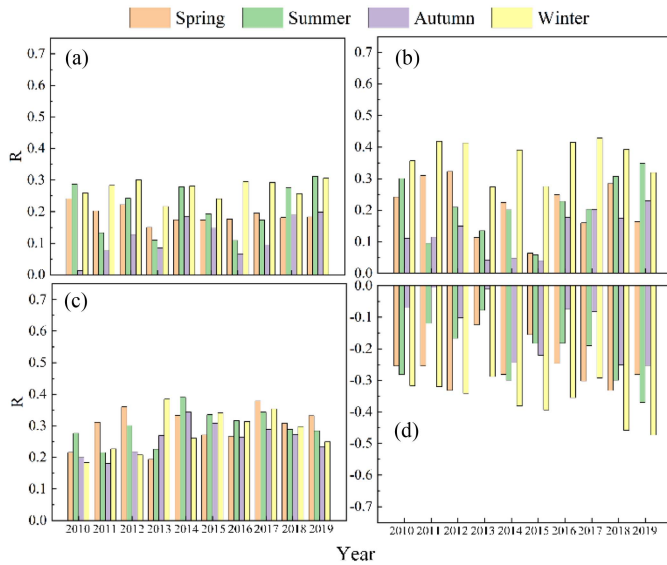


Fig. 12. Correlation analysis between NSATLR and hours of sunshine (a), evaporation (b), wind speed (c), and relative humidity (d) from 2010 to 2019. (a) Hours of Sunshine. (b) Evaporation. (c) Wind Speed. (d) Relative Humidity.

The latent heat caused by evaporation in high altitude areas can change NSATLR. In spring, summer, autumn, and winter of 2010 to 2019, the mean correlation coefficients between evapotranspiration and NSATLR are 0.21, 0.20, 0.13, and 0.37, respectively. The correlations between evapotranspiration and NSATLR are stronger in winter and weaker in autumn.

There is a positive correlation between wind speed and NSATLR. Wind would promote the loss of ground energy and take away the heat in the air. The greater the wind speed, the faster the energy loss in the air. The stronger wind speed can also make NSATLR deeper [23]. In spring, summer, autumn and winter of the years from 2010 to 2019, the mean correlation coefficients between wind speed and NSATLR are 0.29, 0.29, 0.25, and 0.28, respectively. The correlations between wind speed and NSATLR are stronger in spring, summer and winter, and weaker in autumn.

There is a negative correlation between relative humidity and NSATLR. Li et al. [34] found that NSATLR tends to be shallower with higher temperatures and higher relative humidity through the study of NSATLR in China. Shen et al. [17] pointed out that the difference in NSATLR on the northern and southern slopes of Tianshan Mountains is related to factors such as air temperature, relative humidity, and wind speed. In spring, summer, autumn, and winter of the years from 2010 to 2019, the mean correlation coefficients between relative humidity and NSATLR are -0.26 , -0.22 , -0.13 , and -0.36 , respectively. The correlations between relative humidity and NSATLR are stronger in winter and weaker in autumn.

V. DISCUSSION

The MODIS atmospheric product is introduced in this article to establish the NSATLR estimation model, which simplifies the estimation process of remotely sensed NSATLR. Comparison with NSATLR_{in situ} estimated based on meteorological data

shows that the values of RMSE and MBE are within reasonable limits, confirming the reliability of the NSATLR estimation model.

Previous studies were mostly based on meteorological data, showing the temporal characteristics and overall regional variation of the average NSATLR over the TP and its surrounding areas [22], [23], [35]. However, it is still difficult to reflect the spatially continuous distribution pattern of NSATLR in the TP. With the development of remote sensing technology, remotely sensed thermal infrared data provide the possibility to quantitatively obtain the spatially continuous NSATLR. Wang et al. [23] estimated the NSAT of the TP based on the statistical relationship between the MODIS surface temperature and the in situ NSAT. Then, the estimated NSAT combined with elevation data was subjected to regression analysis within a moving window of $10\text{ km} \times 10\text{ km}$, and the spatial distribution of NSATLR in the TP was obtained. The lack of enough elevation difference within the $10\text{ km} \times 10\text{ km}$ window and the lack of correlation between temperature and elevation may produce unrealistic NSATLR. Based on MODIS LST data and in situ NSAT, Zhang et al. [36] estimated NSAT by multiple linear regression method and obtained the NSATLR. It is found that directly calculating the lapse rate of MODIS LST at night can simulate the monthly average NSATLR with high accuracy. These studies have a great dependence on meteorological data. However, the complex topography and climate in the TP may easily lead to large errors in estimating NSAT from surface temperature based only on statistical relationships.

The model proposed in this article is based entirely on the MODIS atmospheric profile product to estimate NSAT, making the model simple and easy to use. In addition, the size of the moving window is continuously changed during the model establishment process to meet required criteria, thus, strictly controlling the input data of the model for more reliable NSATLR estimation. The RMSE and MBE of the obtained NSATLR compared with the NSATLR_{in situ} are within a reasonable range.

The developed NSATLR estimation model has confirmed its applicability in the TP with complex terrain and climate change. In the process of model construction, it is necessary to control the elevation difference of pixels in the moving window to ensure the accuracy of NSATLR. Therefore, the potential application of this model in other areas with little terrain fluctuation remains to be studied. In addition, the parameterization scheme for determining NSAT in this article is based on the troposphere hydrostatic atmospheric assumption. The atmospheric profile extrapolation can reduce the underestimation by hydrostatic interpolation, but there are still some errors. This is because the atmospheric pressure levels used to estimate NSAT is lower than the surface pressure.

VI. CONCLUSION

Accurate spatially continuous NSATLR is useful in a variety of scientific fields, including climate change research, hydrological research, and ecological research. However, due to the complex interaction between the atmosphere and land surface systems, it is far from simple to retrieve NSATLR entirely from

remotely sensed data. In this article, a new NSATLR estimation model has been proposed based on MODIS atmospheric profile product, which is independent of a variety of auxiliary surface variables and meteorological data. At the same time, in the process of model establishment, the size of moving window is constantly changed to meet required criteria to obtain NSATLR with high accuracy.

The results show that in the central and western TP, the NSATLR estimated by remote sensing-based method is underestimated compared with NSATLR_{in situ} estimated by meteorological data and the RMSE is 1.38 °C/km. However, in the eastern of TP, NSATLR is overestimated compared with NSATLR_{in situ}, and the difference between the two is large, with an annual mean RMSE of 2.53 °C/km. According to the time series characteristics of NSATLR and NSATLR_{in situ}, the difference between them is small in the eastern TP, while large in the central and southern TP. This phenomenon may be related to the density of stations, i.e., the number of stations in the eastern TP is far more than that in the central and southern TP.

This article shows that NSATLR in the northern, western, and central TP is deeper than that in the southeast. Overall, the NSATLR of the TP is deeper in spring and winter, and shallower in summer and autumn. There are more inversion phenomena in spring and winter, and less inversion phenomena in summer and autumn. In addition, the correlation analysis between NSATLR and meteorological factors shows that NSATLR is positively correlated with sunshine hours, evapotranspiration and wind speed, and negatively correlated with relative humidity. Among them, NSATLR is highly correlated with wind speed and relative humidity. In winter, NSATLR is more sensitive to changes in meteorological factors than in autumn, and is more susceptible to them.

The simplicity, easy availability of input parameters, the independence from meteorological data, and the excellence of estimation results are the outstanding advantages of the developed NSATLR estimation model in this article. The NSATLR based on the developed model would help to better examine the mountain climate and provide more accurate parameters for glacier, hydrological and ecological simulation.

ACKNOWLEDGMENT

The authors would like to thank the providers of the datasets used in this article, including the National Aeronautics and Space Administration for MODIS data, China Meteorological Administration for the meteorological data, and Shuttle Radar Topography Mission for the digital elevation model and also like to thank insightful comments of the anonymous reviewers.

REFERENCES

- [1] G. Michlmayr et al., "Application of the Alpine 3D model for glacier mass balance and glacier runoff studies at Goldbergkees, Austria," *Hydrological Processes*, vol. 22, no. 19, pp. 3941–3949, Sep. 2008, doi: [10.1002/hyp.7102](https://doi.org/10.1002/hyp.7102).
- [2] H. Gao, X. He, B. Ye, and J. Pu, "Modeling the runoff and glacier mass balance in a small watershed on the Central Tibetan Plateau, China, from 1955 to 2008: Modeling runoff and glacier variation in a basin on Tibetan Plateau," *Hydrological Processes*, vol. 26, no. 11, pp. 1593–1603, May 2012, doi: [10.1002/hyp.8256](https://doi.org/10.1002/hyp.8256).
- [3] W. W. Immerzeel, L. P. H. van Beek, M. Konz, A. B. Shrestha, and M. F. P. Bierkens, "Hydrological response to climate change in a glacierized catchment in the Himalayas," *Climatic Change*, vol. 110, no. 3/4, pp. 721–736, Feb. 2012, doi: [10.1007/s10584-011-0143-4](https://doi.org/10.1007/s10584-011-0143-4).
- [4] T. R. Blandford, K. S. Humes, B. J. Harshburger, B. C. Moore, V. P. Walden, and H. Ye, "Seasonal and synoptic variations in near-surface air temperature lapse rates in a mountainous basin," *J. Appl. Meteorol. Climatol.*, vol. 47, no. 1, pp. 249–261, Jan. 2008, doi: [10.1175/2007JAMC1565.1](https://doi.org/10.1175/2007JAMC1565.1).
- [5] W. Wang et al., "All-weather near-surface air temperature estimation based on satellite data over the Tibetan Plateau," *IEEE J. Sel. Topics Appl. Earth Observ. Remote Sens.*, vol. 15, pp. 3340–3350, 2022, doi: [10.1109/JS-TARS.2022.3161800](https://doi.org/10.1109/JS-TARS.2022.3161800).
- [6] L. Ding, J. Zhou, X. Zhang, S. Liu, and R. Cao, "Downscaling of surface air temperature over the Tibetan Plateau based on DEM," *Int. J. Appl. Earth Observ. Geoinf.*, vol. 73, pp. 136–147, Dec. 2018, doi: [10.1016/j.jag.2018.05.017](https://doi.org/10.1016/j.jag.2018.05.017).
- [7] M. Du, M. Zhang, S. Wang, X. Zhu, and Y. Che, "Near-surface air temperature lapse rates in Xinjiang, Northwestern China," *Theor. Appl. Climatol.*, vol. 131, no. 3/4, pp. 1221–1234, Feb. 2018, doi: [10.1007/s00704-017-2040-x](https://doi.org/10.1007/s00704-017-2040-x).
- [8] S. J. Marshall, M. J. Sharp, D. O. Burgess, and F. S. Anslow, "Near-surface-temperature lapse rates on the prince of Wales Icefield, Ellesmere Island, Canada: Implications for regional downscaling of temperature," *Int. J. Climatol.*, vol. 27, no. 3, pp. 385–398, Mar. 2007, doi: [10.1002/joc.1396](https://doi.org/10.1002/joc.1396).
- [9] L. Petersen and F. Pellicciotti, "Spatial and temporal variability of air temperature on a melting glacier: Atmospheric controls, extrapolation methods and their effect on melt modeling, Juncal Norte Glacier, Chile," *J. Geophysical Res., Atmospheres*, vol. 116, Dec. 2011, Art. no. D23109, doi: [10.1029/2011JD015842](https://doi.org/10.1029/2011JD015842).
- [10] C. Richard and D. J. Gratton, "The importance of the air temperature variable for the snowmelt runoff modelling using the SRM," *Hydrological Processes*, vol. 15, no. 18, pp. 3357–3370, Dec. 2001, doi: [10.1002/hyp.1031](https://doi.org/10.1002/hyp.1031).
- [11] A. S. Gardner et al., "Near-surface temperature lapse rates over arctic glaciers and their implications for temperature downscaling," *J. Climate*, vol. 22, no. 16, pp. 4281–4298, Aug. 2009, doi: [10.1175/2009JCLI2845.1](https://doi.org/10.1175/2009JCLI2845.1).
- [12] D. B. Kattel, T. Yao, W. Yang, Y. Gao, and L. Tian, "Comparison of temperature lapse rates from the northern to the southern slopes of the Himalayas," *Int. J. Climatol.*, vol. 35, no. 15, pp. 4431–4443, Dec. 2015, doi: [10.1002/joc.4297](https://doi.org/10.1002/joc.4297).
- [13] W. W. Immerzeel, L. Petersen, S. Ragetti, and F. Pellicciotti, "The importance of observed gradients of air temperature and precipitation for modeling runoff from a glacierized watershed in the Nepalese Himalayas," *Water Resour. Res.*, vol. 50, no. 3, pp. 2212–2226, Mar. 2014, doi: [10.1002/2013WR014506](https://doi.org/10.1002/2013WR014506).
- [14] R. Ojha, "Assessing seasonal variation of near surface air temperature lapse rate across India: Seasonal variation of near surface air temperature lapse rate," *Int. J. Climatol.*, vol. 37, no. 8, pp. 3413–3426, Jun. 2017, doi: [10.1002/joc.4926](https://doi.org/10.1002/joc.4926).
- [15] X. Li, L. Wang, D. Chen, K. Yang, B. Xue, and L. Sun, "Near-surface air temperature lapse rates in the mainland China during 1962–2011: Lapse rates in China during 1962–2011," *J. Geophysical Res., Atmospheres*, vol. 118, no. 14, pp. 7505–7515, Jul. 2013, doi: [10.1002/jgrd.50553](https://doi.org/10.1002/jgrd.50553).
- [16] D. B. Gao, T. Yao, K. Yang, L. Tian, G. Yang, and D. Joswiak, "Temperature lapse rate in complex mountain terrain on the southern slope of the central Himalayas," *Theor. Appl. Climatol.*, vol. 113, no. 3/4, pp. 671–682, Aug. 2013, doi: [10.1007/s00704-012-0816-6](https://doi.org/10.1007/s00704-012-0816-6).
- [17] Y.-J. Shen, Y. Shen, J. Goetz, and A. Brenning, "Spatial-temporal variation of near-surface temperature lapse rates over the Tianshan Mountains, central Asia: Variations of lapse rates," *J. Geophysical Res., Atmospheres*, vol. 121, no. 23, pp. 14,006–14,017, Dec. 2016, doi: [10.1002/2016JD025711](https://doi.org/10.1002/2016JD025711).
- [18] Y. He and K. Wang, "Contrast patterns and trends of lapse rates calculated from near-surface air and land surface temperatures in China from 1961 to 2014," *Sci. Bull.*, vol. 65, no. 14, pp. 1217–1224, Jul. 2020, doi: [10.1016/j.scib.2020.04.001](https://doi.org/10.1016/j.scib.2020.04.001).
- [19] D. B. Kattel, T. Yao, K. Yang, L. Tian, G. Yang, and D. Joswiak, "Temperature lapse rate in complex mountain terrain on the southern slope of the central Himalayas," *Theor. Appl. Climatol.*, vol. 113, no. 3/4, pp. 671–682, Aug. 2013, doi: [10.1007/s00704-012-0816-6](https://doi.org/10.1007/s00704-012-0816-6).
- [20] Y. Li, Z. Zeng, L. Zhao, and S. Piao, "Spatial patterns of climatological temperature lapse rate in mainland China: A multi-time scale investigation," *J. Geophysical Res., Atmospheres*, vol. 120, no. 7, pp. 2661–2675, Apr. 2015, doi: [10.1002/2014JD022978](https://doi.org/10.1002/2014JD022978).
- [21] X. Guo, L. Wang, and L. Tian, "Spatio-temporal variability of vertical gradients of major meteorological observations around the Tibetan Plateau," *Int. J. Climatol.*, vol. 36, no. 4, pp. 1901–1916, Mar. 2016, doi: [10.1002/joc.4468](https://doi.org/10.1002/joc.4468).

- [22] D. B. Kattel, T. Yao, and P. K. Panday, "Near-surface air temperature lapse rate in a humid mountainous terrain on the southern slopes of the eastern Himalayas," *Theor. Appl. Climatol.*, vol. 132, no. 3/4, pp. 1129–1141, May 2018, doi: [10.1007/s00704-017-2153-2](https://doi.org/10.1007/s00704-017-2153-2).
- [23] Y. Wang, L. Wang, X. Li, and D. Chen, "Temporal and spatial changes in estimated near-surface air temperature lapse rates on Tibetan Plateau," *Int. J. Climatol.*, vol. 38, no. 7, pp. 2907–2921, Jun. 2018, doi: [10.1002/joc.5471](https://doi.org/10.1002/joc.5471).
- [24] F. Huang et al., "Air temperature estimation with MODIS data over the Northern Tibetan Plateau," *Adv. Atmospheric Sci.*, vol. 34, no. 5, pp. 650–662, May 2017, doi: [10.1007/s00376-016-6152-5](https://doi.org/10.1007/s00376-016-6152-5).
- [25] Y. Rao et al., "Estimating daily average surface air temperature using satellite land surface temperature and top-of-atmosphere radiation products over the Tibetan Plateau," *Remote Sens. Environ.*, vol. 234, Dec. 2019, Art. no. 111462, doi: [10.1016/j.rse.2019.111462](https://doi.org/10.1016/j.rse.2019.111462).
- [26] X. Zhang, S. Liang, G. Zhou, H. Wu, and X. Zhao, "Generating global land surface satellite incident shortwave radiation and photosynthetically active radiation products from multiple satellite data," *Remote Sens. Environ.*, vol. 152, pp. 318–332, Sep. 2014, doi: [10.1016/j.rse.2014.07.003](https://doi.org/10.1016/j.rse.2014.07.003).
- [27] W. Zhu, A. Lú, S. Jia, J. Yan, and R. Mahmood, "Retrievals of all-weather daytime air temperature from MODIS products," *Remote Sens. Environ.*, vol. 189, pp. 152–163, Feb. 2017, doi: [10.1016/j.rse.2016.11.011](https://doi.org/10.1016/j.rse.2016.11.011).
- [28] P. F. Flores and M. F. Lillo, "Simple air temperature estimation method from modis satellite images on a regional scale," *Chilean J. Agricultural Res.*, vol. 70, no. 3, pp. 436–445, Sep. 2010.
- [29] G. Bisht and R. L. Bras, "Estimation of net radiation from the MODIS data under all sky conditions: Southern great plains case study," *Remote Sens. Environ.*, vol. 114, no. 7, pp. 1522–1534, Jul. 2010, doi: [10.1016/j.rse.2010.02.007](https://doi.org/10.1016/j.rse.2010.02.007).
- [30] W. Wang, S. Liang, and T. Meyers, "Validating MODIS land surface temperature products using long-term nighttime ground measurements," *Remote Sens. Environ.*, vol. 112, no. 3, pp. 623–635, Mar. 2008, doi: [10.1016/j.rse.2007.05.024](https://doi.org/10.1016/j.rse.2007.05.024).
- [31] S. Li, T. Yao, L. Tian, and P. Wang, "Seasonal transition characteristics of the westerly jet: Study based on field observations at an altitude of 6900 m on the Mt. Xixiabangma Dasuopu glacier," *Chin. Sci. Bull.*, vol. 56, no. 18, pp. 1912–1920, Jun. 2011, doi: [10.1007/s11434-011-4508-x](https://doi.org/10.1007/s11434-011-4508-x).
- [32] J. R. Minder, P. W. Mote, and J. D. Lundquist, "Surface temperature lapse rates over complex terrain: Lessons from the Cascade Mountains," *J. Geophys. Res.*, vol. 115, no. D14, Jul. 2010, Art. no. D14I22, doi: [10.1029/2009JD013493](https://doi.org/10.1029/2009JD013493).
- [33] X. Guo, L. Wang, and L. Tian, "Spatio-temporal variability of vertical gradients of major meteorological observations around the Tibetan Plateau: Vertical gradients of meteorological observations," *Int. J. Climatol.*, vol. 36, no. 4, pp. 1901–1916, Mar. 2016, doi: [10.1002/joc.4468](https://doi.org/10.1002/joc.4468).
- [34] Y. Li, Z. Zeng, L. Zhao, and S. Piao, "Spatial patterns of climatological temperature lapse rate in mainland China: A multi-time scale investigation," *J. Geophysical Res.: Atmospheres*, vol. 120, no. 7, pp. 2661–2675, Apr. 2015, doi: [10.1002/2014JD022978](https://doi.org/10.1002/2014JD022978).
- [35] Y. He and K. Wang, "Contrast patterns and trends of lapse rates calculated from near-surface air and land surface temperatures in China from 1961 to 2014," *Sci. Bull.*, vol. 65, no. 14, pp. 1217–1224, Jul. 2020, doi: [10.1016/j.scib.2020.04.001](https://doi.org/10.1016/j.scib.2020.04.001).
- [36] H. Zhang, F. Zhang, G. Zhang, T. Che, and W. Yan, "How accurately can the air temperature lapse rate over the Tibetan Plateau be estimated from modis LSTs?," *J. Geophysical Res.: Atmospheres*, vol. 123, no. 8, pp. 3943–3960, Apr. 2018, doi: [10.1002/2017JD028243](https://doi.org/10.1002/2017JD028243).

Hailing Zhong is currently working toward the Graduate degree in surveying and mapping science and technology with the University of Electronic Science and Technology of China, Chengdu, China.

Her research interests include remote sensing and surface temperature, as well as near-surface temperature.

Ji Zhou (Senior Member, IEEE) received the B.S. degree in geographic information systems from Nanjing University, Nanjing, China, in 2005, and the Ph.D. degree in remote sensing from Beijing Normal University, Beijing, China, in 2010.

He was a Visiting Ph.D. Student with the Department of Geography, University of Western Ontario, London, ON, Canada, from 2008 to 2009. From 2015 to 2016, he was an International Research Fellow at European Space Agency, Rome, Italy. From January to February 2020, he was a Senior Visiting Scholar with the Department of Geographical Sciences, University of Maryland, College Park, MD, USA. He is currently a Professor with the School of Resources and Environment, University of Electronic Science and Technology of China, Chengdu, China. His research interests include thermal and passive microwave remote sensing of land surfaces.

Wenbin Tang received the M.S. degree in school of earth sciences with Chengdu university of Technology, Chengdu, China, in 2021. He is currently working toward the Ph.D. degree with the University of Electronic Science and Technology of China, Chengdu, China.

His research interest includes all-weather surface temperature integration

Guiyun Zhou received the B.S. degree in physical geography and M.S. degree in geographic information science with the Peking University, Beijing, China, in 1999 and 2002, respectively, and he received the Ph.D. degree in geography from Louisiana State University, Baton Rouge, LA, USA, in 2006.

He is currently a Professor with the School of Resources and Environment, University of Electronic Science and Technology of China, Chengdu, China. His research interests include spatial modeling, remote sensing image processing, and 3-D modeling.

Ziwei Wang received the master's degree in surveying and mapping in 2022 from the University of Electronic Science and Technology of China, Chengdu, China, where he is currently working toward the Ph.D. degree in information and communication engineering.

His major research interests include UAV remote sensing in agriculture, remote-sensing image processing, and land surface parameter retrieval.

Wei Wang received the M.S. degree in surveying and mapping engineering with the Chengdu University of Technology, Chengdu, China, in 2020. He is currently working toward the Ph.D. degree in information and communication engineering with the University of Electronic Science and Technology of China, Chengdu, China.

His research interests include the estimating near surface air temperature and downscaling for shortwave radiation.

Yizhen Meng is currently working toward the Graduate degree in mater of engineering with the University of Electronic Science and Technology of China, Chengdu, China.

Her current research interest includes the retrieval and validation of surface parameters.

Jin Ma (Member, IEEE) received the B.S. degree in geographic information systems from the Chengdu University of Technology, Chengdu, China, in 2015, and the Ph.D. degree in information and communication engineering (Remote Sensing) from the University of Electronic Science and Technology of China (UESTC), Chengdu, China, in 2021.

He is currently a Postdoctoral Researcher with the UESTC. His research interest includes the retrieval and validation of land surface temperature.